Submicron rectangular cylinders as atom guides

S. Al-Awfi and M. Babiker
Department of Physics, University of Essex, Colchester, Essex CO4 3SQ, England
(Received 8 June 1998)

The guiding of atoms by laser light is investigated for atoms inside a long hollow cylinder with a rectangular cross section of subwavelength dimensions $a \times b$. The cavity modes are quantized, allowing the position-dependent spontaneous emission rate to be evaluated for an electric dipole inside the cylinder. Useful limits of the spontaneous rate are derived. In particular, results appropriate for the parallel-plate case are recovered when side a of the rectangular cross section becomes large, while side b is kept fixed. In the limit of the small cross section, especially when both a and b are less than λ (the atom electric dipole transition wavelength), the spontaneous emission process is possible only via a few cavity modes. If a cavity mode is now excited with sufficient intensity, the atoms become subject to a transverse dipole potential and an axial dissipative force, both of which vary across the cylinder and are also functions of the atom axial velocity. The dipole potential is responsible for the transverse trapping (and hence the channeling) of atoms at specific regions of the cross section, while the dissipative force controls the axial motion of the channeled atoms. The conditions facilitating atom guiding are explored using typical parameters for sodium atoms in rectangular cylinders of subwavelength dimensions. [S1050-2947(98)07212-6]

PACS number(s): 32.80.Pj, 32.80.Lg, 42.50.Vk

I. INTRODUCTION

In a recent paper [1] we have investigated the dynamics of atoms between conducting parallel plates in which a cavity mode is excited. We have shown that the characteristics of such a system depend on a number of factors, including field intensity, sign and magnitude of the detuning, the dipole orientation, and the type of cavity mode excited. When the cavity dimensions become comparable to a dipole transition wavelength λ, the physics of such a system becomes significantly different from that of atom guiding arrangements considered to date. The question then arises as to how would the details of atom guiding be modified in a cylindrical waveguide of a cross section that typically has subwavelength dimensions.

In this paper we examine atom guiding inside cylindrical waveguides with rectangular cross sections. We concentrate here on this type of cross section for two reasons. First, despite the fact that the electromagnetic modes of a rectangular waveguide are well known, it appears that neither the spontaneous emission rate nor the atom dynamics in this structure have been reported before. Second, the rectangular cross section is a natural extension for the parallel-plate case. In fact, the parallel-plate system is one of the useful asymptotic limits of the cylinder with a rectangular cross section. As we show later, this limit provides a useful check of the calculations.

The significance of atom guides for the emerging field of atom optics has been emphasized in our previous paper [1] and the reader is referred to the introduction of that article for background, especially with regard to different types of atom guide and the status of theory and experiment to date [2–8]. The potential application of atom guides in atomic physics research and in lithography are hinged on the ability to maintain channeling in specific regions of the cross section and the consequent generation of an atomic beam. These requirements depend on the mechanism for confining the atoms in well-defined regions of the cross section as they are guided along the axis. As we emphasized in [1], subwavelength atom guides offer the prospect of single mode operation and of a better control of the effects of spontaneous emission. In this paper we explore these expectations in depth for the case of atoms in rectangular cylinders.

The paper is organized as follows. In Sec. II we outline the procedure leading to the quantized electromagnetic modes inside a rectangular waveguide. This readily facilitates the evaluation of the spontaneous emission rate for an electric dipole within the rectangular guide and the variation of this rate with the dimensions of the cross section. The subwavelength regime is emphasized where only one or two modes are responsible for the spontaneous emission. In Sec. III we illustrate the results by considering the case of sodium atoms in subwavelength waveguides. In Sec. IV we consider atom guiding and begin by examining the dynamics of atoms within the guide and in Sec. V we discuss the effects on the motion when a cavity mode is excited. Section VI contains comments and conclusions.

II. QED IN WAVEGUIDE

The atom guide focused on here is in the form of a rectangular waveguide, as depicted in Fig. 1. As shown in this

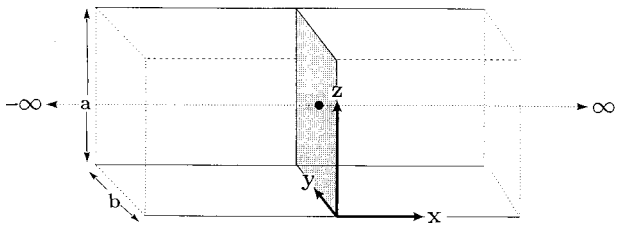

FIG. 1. Schematic drawing of the rectangular waveguide showing the orientation of the Cartesian axes, the axis of the cylinder, and the walls.

figure, a normal cross section is assumed to have the dimensions $a\times b$ and is taken to lie in the y-z plane with the cylinder axis along the x direction, coinciding with the straight line $y=b/2;\ z=a/2$. The guide is bounded by walls arising from the intersection of four planes at $y=0;\ y=b$ and $z=0;\ z=a$, all are assumed to be planar surfaces of perfect conductors which exclude all electromagnetic fields from their interior. The standard electromagnetic boundary conditions apply such that the tangential components of the electric field vector and the magnetic field vector must vanish at every point on all guide walls.

The atom of mass M is characterized by its electric dipole moment $\boldsymbol{\mu}$ of oscillation frequency ω_0 interacting with the electromagnetic modes inside the waveguide. The effective Hamiltonian can be written as

$$H=\frac{P^2}{2M}+U(\mathbf{R})+\hbar\omega_0\pi^\dagger\pi-\boldsymbol{\mu}\cdot\mathbf{E}(\mathbf{R})+H_f, \tag{1}$$

where $\mathbf{P}$ and $\mathbf{R}$ are the momentum and position vectors of the atomic center of mass which is assumed to be subject to a general potential $U(\mathbf{R})$. In the two-level approximation the internal motion of the atom involves only two states: $|e\rangle$, of energy E_e, and $|g\rangle$, of energy E_g, such that $E_e-E_g=\hbar\omega_0$. The operators π and $\pi^\dagger$ are lowering and raising operators for internal atomic states such that $\boldsymbol{\mu}=\langle\boldsymbol{\mu}\rangle_{eg}(\pi+\pi^\dagger)$; $\mathbf{E}$ is the electric field operator and H_f is the electromagnetic field Hamiltonian.

A. Quantized fields

The procedure for enumerating the electromagnetic modes inside the cylinder begins with the solutions of the wave equation for transverse electromagnetic fields. As is well known, there are two types of normal modes: s polarized (TE) and p polarized (TM), both of which satisfy the electromagnetic boundary conditions at the guide walls. The total quantized electric and magnetic field operators are written as follows:

$$\mathbf{E}(x,\mathbf{R}_\perp,t)=\sum_{\eta=(p,s)}\sum_{n,m}\int_{-\infty}^{\infty}dk \times\{a_\eta(k,n,m)\boldsymbol{\mathcal{F}}_\eta(k,n,m,x,\mathbf{R}_\perp,t)+\text{H.c.}\}, \tag{2}$$

$$\mathbf{B}(x,\mathbf{R}_\perp,t)=\sum_{\eta=(p,s)}\sum_{n,m}\int_{-\infty}^{\infty}dk \times\left\{\left(\frac{1}{i\omega(n,m,k)}\right)a_\eta(k,n,m) \times\boldsymbol{\nabla}\times\boldsymbol{\mathcal{F}}_\eta(k,n,m,x,\mathbf{R}_\perp,t)+\text{H.c.}\right\}, \tag{3}$$

where H.c. stands for ''Hermitian conjugate'' and we have expressed the position vector in component form by writing $\mathbf{R}=(x,\mathbf{R}_\perp)$ with x an axial coordinate and $\mathbf{R}_\perp=(y,z)$ a two-dimensional (transverse) position vector in the y-z plane. The operator $a_\eta(k,n,m)$ is the boson operator for the field mode of polarization $\eta(=p,s)$, characterized by the integer quantum numbers n,m and an axial wave vector k. The relevant commutation relations are

$$[a_\eta(k,n,m),a^\dagger_{\eta'}(k',n',m')]=\delta_{\eta\eta'}\delta_{mm'}\delta_{nn'}\delta(k-k'). \tag{4}$$

Finally, $\boldsymbol{\mathcal{F}}_\eta(k,n,m,x,\mathbf{R}_\perp,t)$ are the mode functions for which explicit forms are given below. These vector functions satisfy the wave equation as well as the electromagnetic boundary conditions at the guide walls.

It is convenient to simplify the notation by introducing a compound mode variable Q which stands for the three mode variables (k,n,m). The quantized electric field in Eq. (2) becomes

$$\mathbf{E}(x,\mathbf{R}_\perp,t)=\sum_{\eta=(p,s)}\sum_{Q}\{a_\eta(Q)\boldsymbol{\mathcal{F}}_\eta(Q,x,\mathbf{R}_\perp,t)+\text{H.c.}\}, \tag{5}$$

with a similar equation corresponding to Eq. (3). The sum over Q stands for one integration over k plus two integer sums over n and m. The mode commutation relations are now given by

$$[a_\eta(Q),a^\dagger_{\eta'}(Q')]=\delta_{\eta\eta'}\delta_{QQ'}, \tag{6}$$

where $\delta_{QQ'}$ is interpreted by inspection of the right-hand side of Eq. (4).

The mode functions for the transverse magnetic (TM) modes corresponding to $\eta=p$ (p-polarized modes) emerge in the form [9]

$$\begin{aligned}\boldsymbol{\mathcal{F}}_p(Q,x,\mathbf{R}_\perp,t)=C_p(Q)\{&i\hat{\mathbf{x}}(\kappa_m^2+\kappa_n^2)\sin(\kappa_m y)\sin(\kappa_n z)\\&+\hat{\mathbf{y}}\kappa_m k\cos(\kappa_m y)\sin(\kappa_n z)\\&+\hat{\mathbf{z}}\kappa_n k\sin(\kappa_m y)\cos(\kappa_n z)\}e^{i[kx-\omega(Q)t]},\end{aligned} \tag{7}$$

where carets denote unit vectors; κ_m and κ_n are given by

$$\kappa_m=\frac{m\pi}{b},\quad \kappa_n=\frac{n\pi}{a}. \tag{8}$$

$\omega(Q)$ is the mode frequency satisfying the dispersion relation

$$\omega^2(Q)=c^2\{k^2+\kappa_m^2+\kappa_n^2\}. \tag{9}$$

Finally in Eq. (7), C_p is the p-polarized mode normalization factor given by

$$C_p(Q)=\left(\frac{2\hbar c^2}{AL\epsilon_0\omega(Q)[\kappa_m^2+\kappa_n^2]}\right)^{1/2}, \tag{10}$$

where A is the cross-sectional area of the guide and L is its (large) length.

The second set of electromagnetic modes in the rectangular waveguide is the transverse electric (TE) set of modes corresponding to $\eta=s$ (s-polarized modes). The mode functions for these are given by [9]

$$\mathcal{F}_s(Q,x,\mathbf{R}_\perp,t)=C_s\{-\hat{\mathbf{y}}\kappa_n\cos(\kappa_m y)\sin(\kappa_n z)+\hat{\mathbf{z}}\kappa_m\sin(\kappa_m y)\cos(\kappa_n z)\}e^{i[kx-i\omega(Q)t]}, \tag{11}$$

where C_s is the normalization factor for *s*-polarized modes

$$C_s(Q)=\left(\frac{2\hbar\omega(Q)}{AL\epsilon_0[\kappa_m^2+\kappa_n^2]f_{mn}}\right)^{1/2}, \tag{12}$$

where f_{mn} is such that $f_{01}=\frac{1}{2}=f_{10}$ and $f_{mn}=1$ for m and n satisfying $m\geqslant 1$ and $n\geqslant 1$.

The total Hamiltonian for the electromagnetic fields within the waveguide is

$$H_f=\frac{1}{2}\int_{-\infty}^{\infty}dx\int d^2\mathbf{R}_\perp\left\{\epsilon_0 E^2(x,\mathbf{R}_\perp,t)+\frac{1}{\mu_0}B^2(x,\mathbf{R}_\perp,t)\right\}. \tag{13}$$

The factors C_p and C_s defined in Eqs. (10) and (12) are fixed by the usual quantization requirement that the field Hamiltonian H_f reduces to the canonical form

$$H_f=\frac{1}{2}\sum_{\eta(=p,s)}\sum_Q\hbar\omega(Q)\{a_\eta(Q)a_\eta^\dagger(Q)+a_\eta^\dagger(Q)a_\eta(Q)\}. \tag{14}$$

B. Spontaneous emission

The spontaneous decay rate for an electric dipole $\boldsymbol{\mu}$ situated at an arbitrary point $\mathbf{R}=(x,\mathbf{R}_\perp)$ within the waveguide is evaluated using Fermi's golden rule. By symmetry, this rate cannot depend on the axial coordinate x and we may evaluate it for a dipole situated at an arbitrary point $(0,\mathbf{R}_\perp)$, i.e., at points within the normal cross section in the y-z plane

$$\Gamma(\mathbf{R}_\perp)=\frac{2\pi}{\hbar}\sum_{\eta=(p,s)}\sum_Q|\langle e;\{0\}|-\boldsymbol{\mu}\cdot\mathbf{E}(0,\mathbf{R}_\perp)|g;\{Q,\eta\}\rangle|^2\times\delta(E_e-E_g-\hbar\omega(Q)). \tag{15}$$

As indicated, the transition from the excited internal state $|e\rangle$ to the ground state $|g\rangle$ is effected by the emission of single quanta of waveguide modes with states $|\{Q,\eta\}\rangle$ of frequency $\omega(Q)$ and polarization η. The vacuum state is represented by $|\{0\}\rangle$.

It should be noted that the waveguide frequency spectrum determined by Eq. (9) comprises two sets of discrete branches, one for each type of polarization $\eta=(p,s)$. A frequency branch is labeled by two fixed integers m and n and within any given branch, the frequency varies only with the one-dimensional axial wave vector k. The TE and TM frequency branches for a typical rectangular waveguide are shown in Fig. 2.

Depending on the value of the dipole frequency ω_0, contributions to the emission rate arise from all branches satisfying the condition

$$\omega(Q)\equiv\omega(k,n,m)=\omega_0. \tag{16}$$

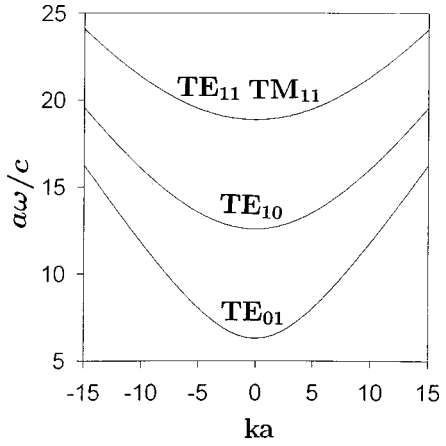

FIG. 2. Dispersion curves showing the TM and TE branches of the guided modes in a cylinder of rectangular cross section with dimensions $a=0.9\lambda$ and $b=0.6\lambda$ where $\lambda=589$ nm.

Since $\omega(k,n,m)$ depends on the guide dimensions a and b entering via κ_m and κ_n, Eq. (16) conceals the dependence on the chosen values of a and b.

Assuming that $b=a$, the ''zone center'' $(k=0)$ frequency separation between the lowest branch TE_{01} corresponding to $m=0$, $n=1$ (or $n=0$, $m=1$) and the adjacent branch $m=1$, $n=1$ is approximately given by

$$\Delta\omega(11-10)=\omega(0,1,1)-\omega(0,1,0)\approx c(\sqrt{2}-1)\frac{\pi}{a}. \tag{17}$$

For $a\approx 1.0\ \mu$m we have $\Delta\omega(11-10)\approx 3.9\times 10^{14}\ \mathrm{s}^{-1}$. Frequency separations of similar orders of magnitudes are obtainable for higher adjacent branches. These frequency separations are therefore quite large for waveguides with dimensions in the micrometer range. From the special case illustrated in Fig. 2 ($a=0.9\lambda$, $b=0.6\lambda$, $\lambda=589$ nm) we see that if the dipole frequency is less than $\omega(0,1,1)$ emission is possible only via the two TE branches. Inspection of Eq. (11) further shows that a dipole oscillating at such a frequency and which is oriented along the axis of the waveguide can couple neither to the electric field of the TE_{01} mode nor to the TE_{10} mode and will therefore not decay spontaneously. On the other hand, the spontaneous decay of a dipole of frequency greater than $\omega(0,1,1)$ will involve both the TE lowest branches as well as the TE_{11} and TM_{11} branches. If, in addition, this dipole is oriented along the axis, only the TM_{11} branch provides a decay channel, since the axial dipole cannot couple to the TE modes. These observations which are significant for submicron waveguides are substantiated further with the calculations of the spontaneous rate, as we now show.

The procedure for the calculation of the total emission rate based on Eq. (15) can be outlined as follows. Contributions from the p and s modes are carried out separately and then combined to yield the total rate. Typically, after evaluating the squared matrix element for a given type of mode, use of the dispersion relation, Eq. (9), facilitates the evaluation of the integral over k involving the δ function. We are then left with two sums over integers m and n and a cutoff condition, Eq. (16), to be satisfied for each evaluation.

C. Contribution of TM modes

Consider first the contribution from the TM modes which involves use of the mode functions defined in Eq. (7). Following the above procedure for the emission rate evaluation for this case culminates in an expression involving sums over m and n. We have at point $\mathbf{R}_\perp=(y,z)$

$$\Gamma_p(\mathbf{R}_\perp)=\sum_m\sum_n\left(\frac{2\mu^2}{\hbar\epsilon_0 a^2 b}\right)\left\{\frac{\langle\mu_x\rangle^2}{\mu^2}G^x_{mn}(\mathbf{R}_\perp)+\frac{\langle\mu_y\rangle^2}{\mu^2}G^y_{mn}(\mathbf{R}_\perp)+\frac{\langle\mu_z\rangle^2}{\mu^2}G^z_{mn}(\mathbf{R}_\perp)\right\}, \quad (18)$$

where μ is the magnitude of the dipole matrix element vector $\langle\boldsymbol{\mu}_{eg}\rangle$, with Cartesian components represented by $\langle\mu_x\rangle$, $\langle\mu_y\rangle$, and $\langle\mu_z\rangle$. The G functions appearing in Eq. (18) are given by

$$G^x_{mn}(\mathbf{R}_\perp)=\frac{\pi^2 H_{mn}}{R_{mn}}\sin^2\left(\frac{m\pi y}{b}\right)\sin^2\left(\frac{n\pi z}{a}\right), \quad (19)$$

$$G^y_{mn}(\mathbf{R}_\perp)=\frac{a^2m^2R_{mn}}{b^2H_{mn}}\cos^2\left(\frac{m\pi y}{b}\right)\sin^2\left(\frac{n\pi z}{a}\right), \quad (20)$$

$$G^z_{mn}(\mathbf{R}_\perp)=\frac{n^2R_{mn}}{H_{mn}}\sin^2\left(\frac{m\pi y}{b}\right)\cos^2\left(\frac{n\pi z}{a}\right), \quad (21)$$

where we have defined R_{mn} and H_{mn} by

$$R_{mn}=(\omega_0^2a^2/c^2-m^2\pi^2a^2/b^2-n^2\pi^2)^{1/2},$$
$$H_{mn}=a^2m^2/b^2+n^2. \quad (22)$$

D. Contribution of TE modes

Similar evaluations leading to the contributions from the s-polarized modes are based on Eq. (11). The results can be written in the form

$$\Gamma_s(\mathbf{R}_\perp)=\sum_m\sum_n\left(\frac{2\mu^2\omega_0^2}{\hbar\epsilon_0c^2bf_{mn}}\right)\times\left\{\frac{\langle\mu_y\rangle^2}{\mu^2}F^y_{mn}(\mathbf{R}_\perp)+\frac{\langle\mu_z\rangle^2}{\mu^2}F^z_{mn}(\mathbf{R}_\perp)\right\}, \quad (23)$$

where F^y_{mn} and F^z_{mn} are given by

$$F^y_{mn}(\mathbf{R}_\perp)=\frac{n^2}{H_{mn}R_{mn}}\cos^2\left(\frac{m\pi y}{b}\right)\sin^2\left(\frac{n\pi z}{a}\right), \quad (24)$$

$$F^z_{mn}(\mathbf{R}_\perp)=\frac{a^2m^2}{b^2H_{mn}R_{mn}}\sin^2\left(\frac{m\pi y}{b}\right)\cos^2\left(\frac{n\pi z}{a}\right). \quad (25)$$

E. Total spontaneous rate

The results in Eqs. (18) and (23), respectively, give the contributions of the TM and the TE modes to the spontaneous emission rate for an electric dipole of frequency ω_0 in an arbitrary rectangular waveguide with a cross section of dimensions $a\times b$.

For a given dipole orientation, the spontaneous emission rate is given by the sum of contributions from the TM and TE set of modes. The results can be written in terms of λ, the free space transition wavelength. For a dipole oriented along the axis we have

$$\Gamma_x(\mathbf{R}_\perp)=\Gamma_0\sum_{m=0}^{[2b/\lambda]}\sum_{n=0}^{[2a/\lambda]}\frac{3\lambda^3}{4\pi^2a^2b}G^x_{mn}(\mathbf{R}_\perp) \quad (26)$$

and for dipoles oriented transversely along the y or z direction, we have

$$\Gamma_{y,z}(\mathbf{R}_\perp)=\Gamma_0\sum_{m=0}^{[2b/\lambda]}\sum_{n=0}^{[2a/\lambda]}\left(\frac{3\lambda}{b}\right)\times\left\{\frac{1}{f_{mn}}F^{y,z}_{mn}(\mathbf{R}_\perp)+\frac{\lambda^2}{4\pi^2a^2}G^{y,z}_{mn}(\mathbf{R}_\perp)\right\}, \quad (27)$$

[In Eqs. (26) and (27) we have used the notation [ ] to indicate the integer part of the bracketed quantity. Also Γ_0 is the corresponding spontaneous rate in free space

$$\Gamma_0=\frac{\mu^2\omega_0^3}{3\pi\hbar\epsilon_0c^3}. \quad (28)$$

These results can now be explored for a typical situation involving a sodium atom in a rectangular waveguide. Our main concern here, however, is with the regime in which a and b take values in the micron range.

Before we consider this regime, it is instructive to check the results using a particularly simple asymptotic limit arising when side a of the cross section increases to infinity with b fixed. As we show next, it is possible to check by explicit calculations that in this limit the contributions from Eqs. (18) and (23) give values for the well-known emission rates for dipoles between parallel plates.

III. SODIUM ATOMS IN MICROGUIDES

For orientation as to orders of magnitude it is instructive to concentrate now on a typical physical situation. We consider the case of a sodium atom and focus on its $3^2s_{1/2}\leftrightarrow 3^2p_{3/2}$ transition ($\lambda=589$ nm). The magnitude of the dipole matrix element associated with this transition is about $\mu=2.6ea_B$, which is consistent with the measured free space lifetime of $\tau_0\approx 16.3$ ns (or $\Gamma_0=6.13\times10^7$ s^{-1}).

Figure 3 shows the spontaneous emission rate for a sodium atom at the center of the cylinder, i.e., at the point $(0,b/2,a/2)$, with the atomic dipole oriented in turn along the three axes ($\xi=x,y,z$). The plots show the ratio emission rate against a/b with b fixed at $b=0.6\lambda$ and for different dipole orientations. In the axial dipole orientation shown in Fig. 3(i) there is a ''cutoff'' value of a below which there is no spontaneous emission. In each case the rate oscillates with increasing a and shows a clear tendency to asymptotically attaining a fixed value at large a.

It is of interest to check that all asymptotic values of the rectangular case obtained for a fixed value of b and large a are consistent with those obtained when the same dipole at the point $y=b/2$ is oriented parallel to two plates separated by a distance $b=0.6\lambda$. The parallel-plate emission rates are

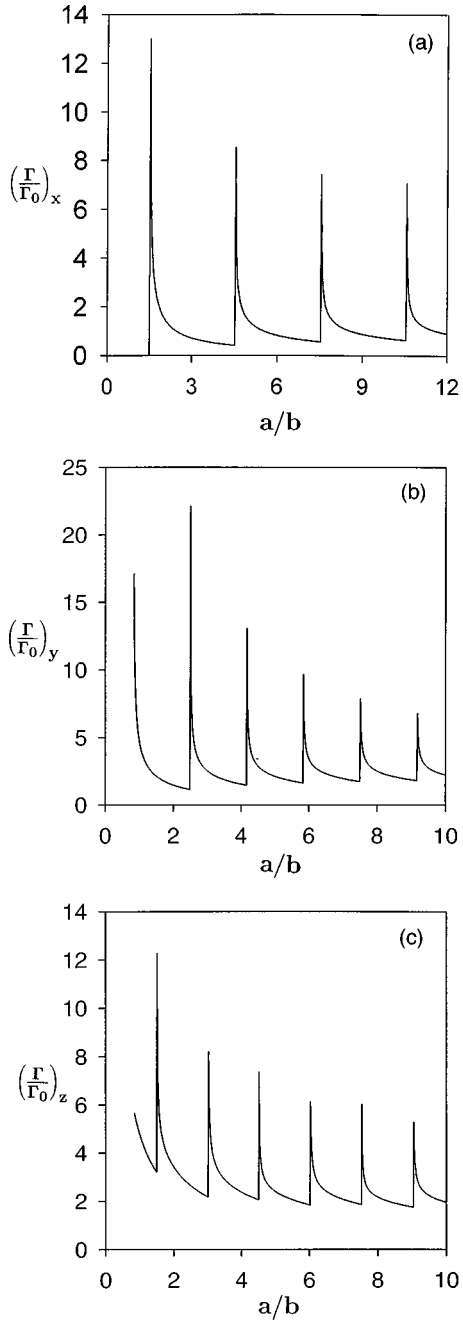

FIG. 3. Total spontaneous emission rate against a/b with b fixed at $b=0.6\ \mu$m for a sodium atom at the center of the cylinder $x=0$; $y=b/2$; $z=a/2$ when the atomic dipole is oriented along the (a) x axis, (b) y axis, and (c) z axis. Here Γ_0 is the free space value of the spontaneous rate.

well known (see, for example, Barton [10] and Hinds [11]). In terms of our choice of axes the emission rate for a dipole oriented parallel to the plates is

$$\Gamma_{\parallel}(y)=\Gamma_0\sum_{n=0}^{[2b/\lambda]}\frac{3\lambda}{4b}\left\{1+\left(\frac{n\lambda}{2b}\right)^2\right\}\sin^2\left(\frac{n\pi}{b}y\right) \quad (29)$$

while for a dipole oriented perpendicular to the plates we have

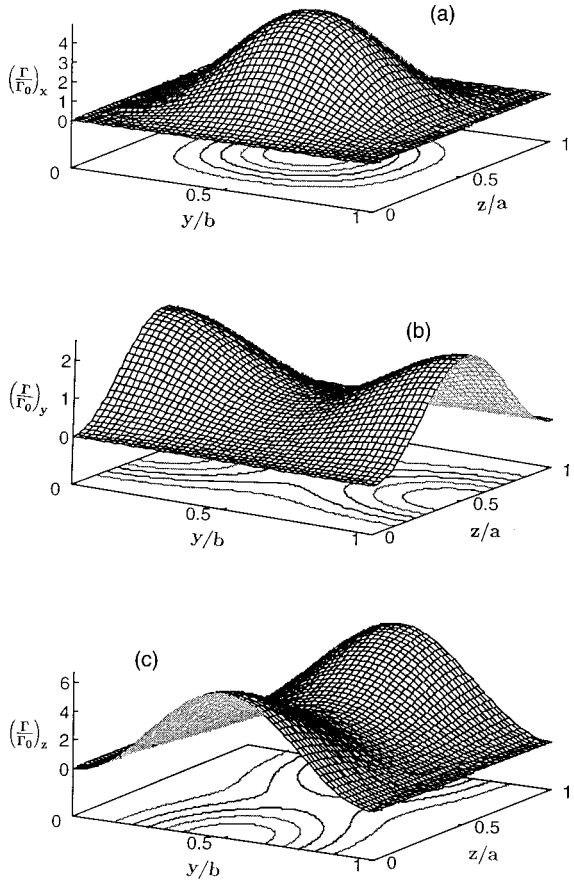

FIG. 4. Distribution and contour plots for the spontaneous emission rate when the dipole matrix element has different orientations (a) along the x axis, (b) along the y axis, and (c) along the z axis. See the text for other assumed parameters.

$$\Gamma_{\perp}(y)=\Gamma_0\left[\frac{3\lambda}{4b}+\sum_{n=1}^{[2b/\lambda]}\frac{3\lambda}{2b}\left\{1-\left(\frac{n\lambda}{2b}\right)^2\right\}\cos^2\left(\frac{n\pi}{b}y\right)\right]. \quad (30)$$

The values obtained from Eqs. (29) and (30) are

$$\Gamma_{\parallel}(y=b/2)=2.118\Gamma_0, \quad \Gamma_{\perp}(y=b/2)=1.25\Gamma_0. \quad (31)$$

The corresponding results emerging from the rectangular guide results in the asymptotic limit $a\to\infty$ must be combined to yield the parallel-plate case. Numerical evaluations in the parallel dipole case confirm that the sum $\Gamma_x^p+\Gamma_z^s+\Gamma_z^p$ evaluated at $(0,b/2,a/2)$ for fixed $b=0.6\lambda$ in the limit of a becoming large converges to $2.118\Gamma_0$, while for the normal dipole case we find that the sum $\Gamma_y^s+\Gamma_y^p$ converges to the value $1.25\Gamma_0$.

Figure 4 shows the distribution and contour plots for the spontaneous emission rate when the dipole matrix element has various orientations. The evaluations are carried out for points spanning the guide cross section and are based on the expressions given in Eqs. (26) and (27). Contributions from individual types of mode are not shown. As a general rule, however, the spontaneous rate is maximum where field components parallel to the dipole matrix element have maximum intensity. It is important to note that, because of the subwavelength dimensions a and b chosen for illustration purposes in Fig. 4, the emission rate distributions arise from at

most three branches of the mode spectrum for a rectangular guide and two for the square guide. This observation is significant for the atom guiding applications to be considered in the next section.

IV. ATOM GUIDING

A. Dynamics

The dynamics of an atom inside the cylinder is modified at the onset of the excitation of a waveguide mode which induces radiation pressure forces of the kinds encountered in laser cooling and trapping (see, for example, Refs. [12–14]). We assume that a mode of the waveguide is excited with a specific compound quantum number $Q \equiv (k,n,m)$, polarization type η, and frequency $\omega(Q)$. However, for convenience, we suppress the mode labels in the following outline derivation of the radiation forces acting on the atom due to this mode.

It is convenient to deal with the fields associated with an excited mode in the classical limit. Hence we may replace the field operators by c numbers and write $a(t) \rightarrow \alpha e^{-i\omega t}$, with a similar expression for $a^{\dagger}$. In the rotating wave approximation the interaction Hamiltonian may then be written as

$$H_{\rm int} = -\boldsymbol{\mu}\cdot\mathbf{E}(\mathbf{R}) = -i\hbar[\tilde{\pi}^{\dagger} f(\mathbf{R}) - \text{H.c.}], \tag{32}$$

where we have set $\tilde{\pi} = \pi e^{i\omega t}$ and introduced the function $f(\mathbf{R})$ by

$$f(\mathbf{R}) = \Omega(\mathbf{R}) e^{i\Theta(\mathbf{R})}. \tag{33}$$

Here $\Omega(\mathbf{R})$ is a Rabi frequency defined by

$$\hbar\Omega(\mathbf{R}) = |\alpha\langle\boldsymbol{\mu}\rangle_{eg}\cdot\boldsymbol{\mathcal{F}}|, \tag{34}$$

with $\boldsymbol{\mathcal{F}}$ the mode vector function, either for an *s*-polarized guide mode or a *p*-polarized one. The forces acting on the atomic center of mass can be derived using the optical Bloch equations for the atomic density matrix elements once we make the semiclassical approximation which allows the gross motion of the atom to be treated classically, while maintaining a quantum treatment for the internal dynamics of the atom. Thus the position and momentum operators of the center of mass may be replaced by their expectation values $\mathbf{R}_0$ and $\mathbf{P}_0$. The density matrix associated with the internal motion of the atom $\rho(t)$ evolves with time according to the well-known relation

$$\frac{d\rho}{dt} = -\frac{i}{\hbar}[H,\rho] + \mathcal{R}\rho, \tag{35}$$

where $\mathcal{R}\rho$ accounts for the relaxation dynamics of the atomic system. By substitution of H and use of the coupling given in Eq. (32), we obtain the following optical Bloch equations for the atomic density matrix elements:

$$\frac{d\rho_{22}}{dt} = -2\Gamma\rho_{22} - f(\mathbf{R}_0)\tilde{\rho}_{12} - f^*(\mathbf{R}_0)\tilde{\rho}_{21}, \tag{36}$$

$$\frac{d\tilde{\rho}_{21}}{dt} = -(\Gamma - i\Delta_0)\tilde{\rho}_{21} + f(\mathbf{R}_0)(\rho_{22} - \rho_{11}), \tag{37}$$

where $\Delta_0 = \omega - \omega_0$ is the detuning of the field frequency from atomic resonance and $\tilde{\rho}_{21} = \langle\tilde{\pi}\rangle$.

The average radiation force acting on the atom is defined as the average rate of change of the atomic momentum, which yields

$$\langle\mathbf{F}\rangle = -\langle\boldsymbol{\nabla} H_{\rm int}\rangle. \tag{38}$$

Substitution of Eq. (32) into Eq. (38) and use of Eq. (33) allows the force to be written as $\langle\mathbf{F}\rangle = \langle\mathbf{F}_{\rm diss}\rangle + \langle\mathbf{F}_{\rm dipole}\rangle$. Here $\langle\mathbf{F}_{\rm diss}\rangle$ is the dissipative force given by

$$\langle\mathbf{F}_{\rm diss}\rangle = -\hbar\boldsymbol{\nabla}\Theta(\mathbf{R}_0)\{\tilde{\rho}_{12}(t) f(\mathbf{R}_0) + \tilde{\rho}_{21}(t) f^*(\mathbf{R}_0)\}, \tag{39}$$

and $\langle\mathbf{F}_{\rm dipole}\rangle$ is the dipole force given by

$$\langle\mathbf{F}_{\rm dipole}\rangle = i\hbar\,\frac{\boldsymbol{\nabla}\Omega(\mathbf{R}_0)}{\Omega(\mathbf{R}_0)}\{\tilde{\rho}_{12}(t) f(\mathbf{R}_0) - \tilde{\rho}_{21}(t) f^*(\mathbf{R}_0)\}. \tag{40}$$

In the adiabatic approximation, the atomic velocity $\mathbf{V} = \mathbf{P}_0/M$ is assumed constant during the time taken for the dipole moment to relax to its steady-state value. The position $\mathbf{R}_0$ of the atom at time t is then given by

$$\mathbf{R}_0 = \mathbf{R} + \mathbf{V}t, \tag{41}$$

where we have redefined $\mathbf{R}$ so that it now denotes the (updated) initial position of the atom. Thus we can write

$$f(\mathbf{R}_0) = f(\mathbf{R} + \mathbf{V}t) \tag{42}$$

$$\simeq f(\mathbf{R}) e^{i\boldsymbol{\nabla}\Theta(\mathbf{R})\cdot\mathbf{V}t}, \tag{43}$$

where we have assumed that the change in the field amplitude is negligible during the time taken for the dipole moment to relax to its steady-state value.

Within the adiabatic approximation, the optical Bloch equations take the form

$$\frac{d\rho_{22}}{dt} = -2\Gamma\rho_{22} - f(\mathbf{R})\hat{\rho}_{12} - f^*(\mathbf{R})\rho_{21}, \tag{44}$$

$$\frac{d\hat{\rho}_{21}}{dt} = -[\Gamma - i\Delta(\mathbf{R},\mathbf{V})]\hat{\rho}_{21} + f(\mathbf{R})(\rho_{22} - \rho_{11}), \tag{45}$$

where the total detuning $\Delta(\mathbf{R},\mathbf{V}) = \Delta_0 - \boldsymbol{\nabla}\Theta(\mathbf{R})\cdot\mathbf{V}$ and $\hat{\rho}_{21} = \tilde{\rho}_{21} e^{-it\mathbf{V}\cdot\boldsymbol{\nabla}\Theta(\mathbf{R})}$. The forces can now be written as

$$\langle\mathbf{F}_{\rm diss}\rangle = -\hbar\boldsymbol{\nabla}\Theta(\mathbf{R})\{\hat{\rho}_{12}(t) f(\mathbf{R}) + \hat{\rho}_{21} f^*(\mathbf{R})\}, \tag{46}$$

$$\langle\mathbf{F}_{\rm dipole}\rangle = i\hbar\,\frac{\boldsymbol{\nabla}\Omega(\mathbf{R})}{\Omega(\mathbf{R})}\{\hat{\rho}_{12}(t) f(\mathbf{R}) - \hat{\rho}_{21}(t) f^*(\mathbf{R})\}. \tag{47}$$

For given initial conditions the solution of the optical Bloch equations (44) and (45) leads formally to the determination of the forces by direct substitution in Eqs. (46) and (47).

Consider first the dissipative force. Setting $\mathbf{R} = (x,\mathbf{R}_{\perp})$ with $\mathbf{R}_{\perp} = (y,z)$, it is easy to show that in the steady state, Eqs. (44)–(46) yield a position-dependent dissipative force associated with the light due to the excited waveguide mode. By symmetry, the force can only depend on the y,z coordi-

nates spanning the cross section. This force is also a function of V_x, the velocity of the atom along the axis of the cylinder, and is always directed along the axis. The explicit form of the dissipative force for a waveguide mode characterized by Q and η is

$$\langle \mathbf{F}_\xi^\eta(Q,\mathbf{R}_\perp)\rangle = 2\hbar\Gamma_\xi(\mathbf{R}_\perp)\Omega_\xi^2(Q,\eta,\mathbf{R}_\perp) \times\left\{\frac{k\hat{\mathbf{x}}}{\Delta^2(Q,V_x)+2\Omega_\xi^2(Q,\eta,\mathbf{R}_\perp)+\Gamma_\xi^2(\mathbf{R}_\perp)}\right\}, \tag{48}$$

where ξ indicates the dipole orientation; $\Delta(Q,V_x)$ is the dynamic detuning, defined by

$$\Delta(Q,V_x)=\omega(Q)-\omega_0-kV_x=\Delta_0(Q)-kV_x. \tag{49}$$

$\Omega_\xi(Q,\eta,\mathbf{R}_\perp)$ is a position-dependent Rabi frequency associated with the cavity mode when the dipole is oriented along the Cartesian ξ direction and is defined by

$$\hbar\Omega_\xi(Q,\eta,\mathbf{R}_\perp)=|\alpha\langle\boldsymbol{\mu}\rangle_{eg}\cdot\boldsymbol{\mathcal{F}}_\eta(Q,\mathbf{R}_\perp)|_\xi, \tag{50}$$

where $\boldsymbol{\mathcal{F}}_\eta$ is either p polarized or s polarized, as given in Eqs. (7) and (11).

In the presence of the same mode, the atom also becomes subject to a light-induced force. In the steady state this is obtainable from Eqs. (44), (45), and (47) and the result is derivable from the dipole potential associated with the mode. This, too, depends on the dipole orientation as well as the type of cavity mode and can be written as

$$U_\xi^\eta(Q,\mathbf{R}_\perp)=\frac{\hbar\Delta(Q,V_x)}{2}\ln\left[1+\frac{2\Omega_\xi^2(Q,\eta,\mathbf{R}_\perp)}{[\Delta^2(Q,V_x)+\Gamma_\xi^2(\mathbf{R}_\perp)]}\right]. \tag{51}$$

The classical motion of the center of mass of the atom is determined by the solution of the equation of motion

$$M\left(\frac{d^2\mathbf{R}}{dt^2}\right)_\xi=\langle\mathbf{F}_\xi^\eta(Q,\mathbf{R}_\perp)\rangle-\boldsymbol{\nabla}U_\xi^\eta(Q,\mathbf{R}_\perp). \tag{52}$$

We have not included the van der Waals and Casimir-Polder potentials in the above equations of motion. The role of these potentials for atoms in cavities has been clarified both theoretically [1] and experimentally [15–17]; in particular, they are known to be effective only at relatively short distances from planar surfaces. Here we ignore the influence of the van der Waals potential appropriate for subwavelength dimensions, since our main concern is with the atom channeling effects that take place in regions of the cylinder cross section that are far removed from surfaces, specifically in the vicinity of the cylinder axis.

Since $\langle\mathbf{F}_\xi^\eta\rangle$ can be written as $\langle F_\xi^\eta\rangle\hat{\mathbf{x}}$ (and so always points in a direction parallel to the cylinder axis), the equation of motion (52) decouples naturally into two separate equations, corresponding to the axial and transverse components of the atom position vector $\mathbf{R}=(x,\mathbf{R}_\perp)$. We have

$$M\left(\frac{d^2x}{dt^2}\right)_\xi=\langle F_\xi^\eta(Q,\mathbf{R}_\perp)\rangle, \tag{53}$$

$$M\left(\frac{d^2\mathbf{R}_\perp}{dt^2}\right)_\xi=-\boldsymbol{\nabla}U_\xi^\eta(Q,\mathbf{R}_\perp). \tag{54}$$

Note that the axial force is independent of x and only depends on $\mathbf{R}_\perp$ as parameter. In fact Eq. (53) can be written entirely as a first order differential equation in $V_x(t)$. On the other hand V_x appears as a parameter in Eq. (54) due to the dependence of $U_\xi^\eta(Q,\mathbf{R}_\perp)$ on $\Delta(Q,V_x)$.

B. Axial motion

The axial motion follows from the solution of Eq. (53) which may be written as

$$M\frac{dV_x}{dt}=2\hbar\Gamma_\xi\Omega_\xi^2(Q,\eta,\mathbf{R}_\perp) \times\left\{\frac{k}{[\Delta_0(Q)-kV_x]^2+2\Omega_\xi^2(Q,\eta,\mathbf{R}_\perp)+\Gamma_\xi^2(\mathbf{R}_\perp)}\right\}. \tag{55}$$

We assume that the mode $(Q,\ \eta)$ is excited at $t=0$ when the atom is stationary $[V_x(t=0)=0]$ at the space point $(0,\mathbf{R}_\perp)$. The transverse coordinates $\mathbf{R}_\perp=(y,z)$ appear on the right-hand side as parameters and, so Eq. (55) can be integrated straightforwardly. At time $t>0$ the axial velocity emerges from the solution of the equation

$$\beta_1V_x^3+\beta_2V_x^2+\beta_3V_x=t, \tag{56}$$

where the β coefficients are given by

$$\beta_1=-\frac{\beta_2k}{3\Delta_0}=\frac{k^2\Gamma_0M}{3F_0\Omega^2\Gamma},\quad \beta_3=\frac{\Gamma_0M(\Delta_0^2+2\Omega^2+\Gamma^2)}{\Gamma F_0\Omega^2}. \tag{57}$$

We have suppressed the ξ, Q, and η labels for convenience and have introduced $F_0=2\hbar k\Gamma_0$ as a suitable scaling force for this system.

The axial distance $x(t)$ traveled by the atom at time t follows straightforwardly after one further integration

$$x(t)=\int_0^t V_x(t)dt. \tag{58}$$

With the help of Eq. (56) the above equation yields

$$x(t)=\tfrac{3}{4}\beta_1V_x^4+\tfrac{2}{3}\beta_2V_x^3+\tfrac{1}{2}\beta_3V_x^2. \tag{59}$$

Thus $V_x(t)$ and $x(t)$ can be determined once the parameters needed to define the β coefficients are known. The typical parameters for the axial motion are governed by the transverse motion, as we now discuss.

C. Transverse motion

The principal requirement of atom guiding is that the dipole potential given by Eq. (51) be a trapping potential, which is only possible for negative $\Delta_0(Q)$. The second requirement is that the depth of this potential be sufficient to

provide several vibrational states for the atom. In order to illustrate these points we focus on a typical physical situation.

We consider sodium atoms and the dipole transition at $\lambda = 589$ nm. We assume that a specific waveguide mode is excited by a laser with intensity comparable to that used by Renn *et al.* [8] in their experiment $I \approx 10^7$ W m^{-2}. The corresponding free space Rabi frequency is

$$\Omega_0 = \left(\frac{\mu^2 I}{2\hbar^2 \epsilon_0 c} \right)^{1/2} \approx 8.56 \times 10^9 \ \text{s}^{-1}. \tag{60}$$

For the dimensions of the rectangular cross section we take values in the subwavelength range as follows:

$$a = 0.9\lambda, \quad b = 0.6\lambda \tag{61}$$

and for the detuning we assume the value

$$\Delta_0(Q) = \omega_0 - \omega(Q) = -6.0 \times 10^2 \Gamma_0 \approx -36.78 \ \text{GHz}. \tag{62}$$

It is easy to check that this Δ_0 is much smaller than the mode spacing for the waveguide of dimensions a and b, as chosen in Eq. (61).

Finally, we make use of two scaling parameters: a scaling force F_0 which was encountered earlier [see Eq. (57)] and a scaling potential energy U_0. With integers m, n known, $\Delta_0(Q)$ defined in Eq. (62), and with ω_0 corresponding to $\lambda = 589$ nm, it is straightforward to deduce the magnitude of the axial wave vector k using Eq. (9). The scaling parameter F_0 for the cylinder dimensions in Eq. (61) depends on k and for $n = 1 = m$ is given by

$$F_0 = 2\hbar k \Gamma_0 \approx 2.33 \times 10^{-20} \ \text{N} \tag{63}$$

while for the scaling potential energy U_0 we write

$$U_0 = \tfrac{1}{2}\hbar \Gamma_0 = 3.23 \times 10^{-27} \ \text{J} \approx 4.9 \ \text{MHz}. \tag{64}$$

In the figures below, which are all concerned with the case $n = 1 = m$, force is measured in units of F_0 and potential energy in units of U_0.

D. Dipole along axis

With the dipole oriented along the axis and with the TM_{11} mode excited we have a position-dependent Rabi frequency given by

$$\Omega_x(k,1,1,p,\mathbf{R}_\perp) = \Omega_0 \left(\frac{2c}{\omega_0} \right) \left(\frac{\pi^2}{b^2} + \frac{\pi^2}{a^2} \right)^{1/2} \sin \frac{\pi y}{b} \sin \frac{\pi z}{a}. \tag{65}$$

With the dipole oriented along the axis and in a situation corresponding to the above choice of parameters, a dissipative force field given by Eq. (48) is set up with spatial distribution within a cross section of the guide as shown in Fig. 5. It can be seen from this figure that atoms located at the center of the guide experience the strongest force along the axis. The corresponding profile of the dipole potential $U_x^p(\mathbf{R}_\perp)$ is depicted in Fig. 6(a). It can be deduced from this figure that, from a quantum-mechanical point of view, solutions of the two-dimensional Schrödinger equation with

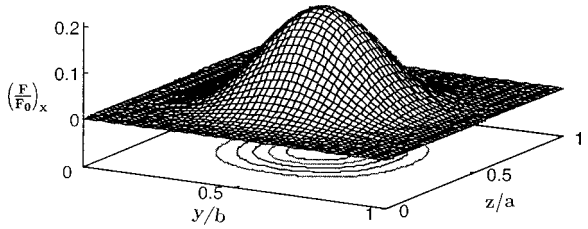

FIG. 5. Spatial distribution within a normal cross section of the quasistatic dissipative force acting on a sodium atom when the TM_{11} mode is excited. Here the electric dipole matrix element is axial; see the text in Sec. IV for the parameters used.

$U_x^p(\mathbf{R}_\perp)$ as potential must exist. In the ground state, the atomic wave function peaks in the vicinity of the central minimum associated with the dipole potential. It can be seen from Fig. 6(b) that for the parameters assumed above, the central well depth is approximately $220U_0 \approx 1.034$ GHz. This is sufficiently deep to allow several quasiharmonic trapping (vibrational) states. The vibrational frequency $\delta\omega_{11}$ can be estimated simply using the parabolic approximation. We find

$$\delta\omega_{11} = \left\{ \frac{2}{M} \frac{d^2}{dz^2} U_x^p(0,b/2,z) \right\}_{z=a/2}^{1/2}. \tag{66}$$

We have explicitly,

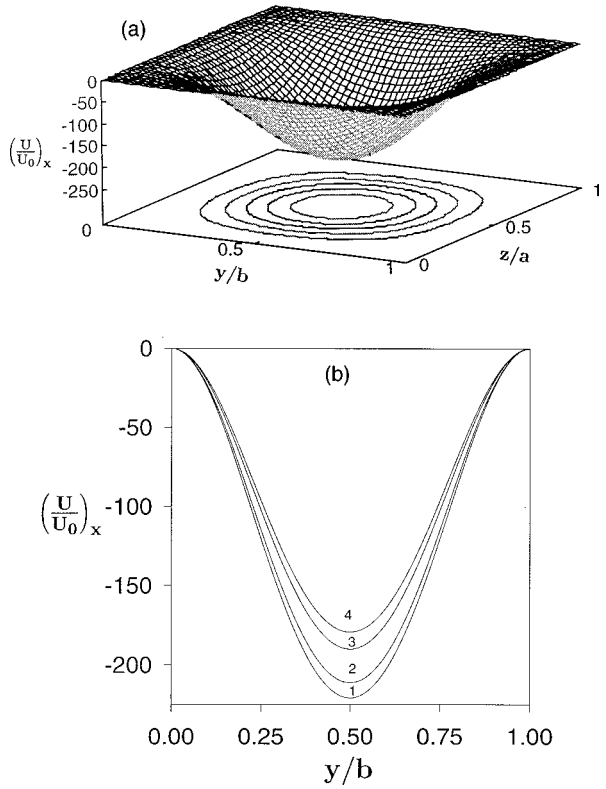

FIG. 6. (a) The potentials of the sodium atom in the rectangular waveguide under the conditions of Fig. 5 when the dipole is along the cylinder axis. (b) Variation of the potential within a central cross section $z = a/2$ for a fixed $b = 0.6\lambda$ and increasing values of a. The labels 1–4 correspond, respectively, to the values $a = 0.9\lambda$, 2.1λ, 2.9λ, and 3.9λ.

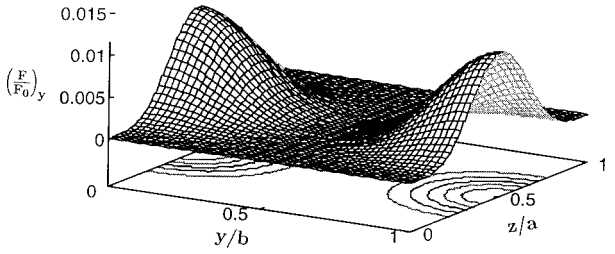

FIG. 7. Spatial distribution in a normal cross section of the quasistatic dissipative force acting on a sodium atom when the TM_{11} mode is excited. Here the electric dipole matrix element is oriented (transversely) along the y axis. See the text in Sec. IV for the parameters used.

$$\delta\omega_{11}=\left(\frac{4\hbar\pi^2\Omega^2\Delta}{(\Delta^2+2\Omega^2)a^2M}\right)^{1/2}_{y=b/2,z=a/2}. \tag{67}$$

It is not difficult to check that with the above parameter values for sodium in the TM_{11} mode within the rectangular waveguide system described above we have

$$\delta\omega_{11}\approx 3.54\times 10^7\ \ \mathrm{s}^{-1}. \tag{68}$$

The precise details of the vibrational energy levels can be obtained straightforwardly by the numerical solution of the two-dimensional Schrödinger equation involving the full $U_x^p(\mathbf{R}_\perp, V_x)$ potential.

The relatively deep potential well in the case of a rectangular cylinder arises from the tight confinement in two spatial directions. If one of the dimensions (side a) is gradually increased while the other (side b) is kept fixed we should approach the parallel-plate limit. That this is indeed the case is shown in Fig. 6(b) where the reduction in the depth of the well for a fixed $b=0.6\lambda$ is achieved by a successive increase in the value of side a. In the limit of large a we expect the results to converge to those appropriate for the parallel-plate case [1].

E. Dipole transverse to axis

With the dipole vector in a plane parallel to the normal cross section, i.e., transverse to the axis and the TM_{11} mode excited, the relevant dipole orientation is either along the y axis or along the z axis. The corresponding Rabi frequencies are given by

$$\Omega_y(k,1,1,p,\mathbf{R}_\perp)=\Omega_0\left(\frac{2ck\pi}{b\omega_0}\right)\left(\frac{\pi^2}{b^2}+\frac{\pi^2}{a^2}\right)^{-(1/2)} \times\cos\frac{\pi y}{b}\sin\frac{\pi z}{a}, \tag{69}$$

$$\Omega_z(k,1,1,p,\mathbf{R}_\perp)=\Omega_0\left(\frac{2ck\pi}{a\omega_0}\right)\left(\frac{\pi^2}{b^2}+\frac{\pi^2}{a^2}\right)^{-(1/2)} \times\sin\frac{\pi y}{b}\cos\frac{\pi z}{a}. \tag{70}$$

The quasistatic dissipative force corresponding to the same choice of parameters as in the preceding subsection is shown in Fig. 7 for a dipole oriented (transversely) along the y axis

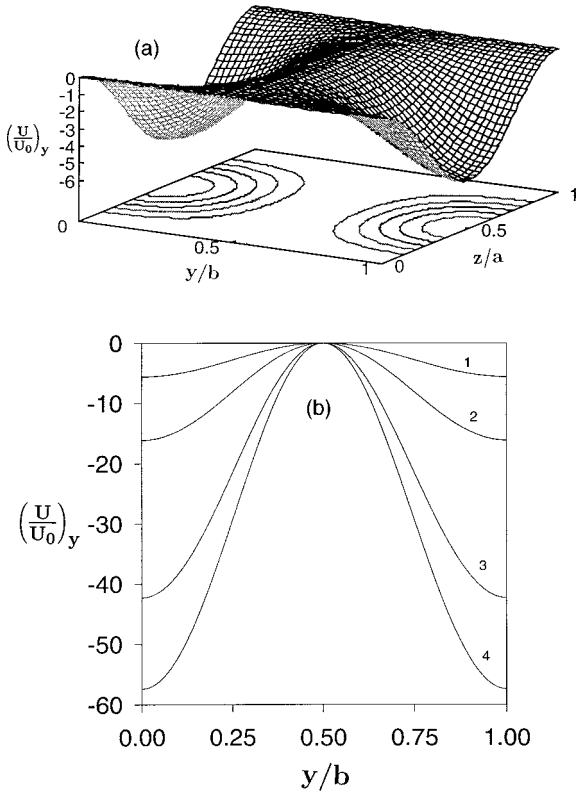

FIG. 8. (a) Potential of the sodium atom in the rectangular guide under the conditions of Fig. 7 for dipole along the y direction; (b) change in the potential depth and profile for a fixed $b=0.6\lambda$ and varying a. The labels 1 to 4 correspond, respectively, to the values $a=0.9\lambda$, 2.1λ, 2.9λ, and 3.9λ.

and the corresponding potential profile $U_y^p(\mathbf{R}_\perp)$ is depicted in Fig. 8(a). The case of a dipole oriented transversely along the z axis yields very similar results (with interchange of axes). In contrast to the case of axial dipole orientation, the dipole potential for the transverse case has no minimum at the center of the guide. It, in fact, tends to attract the atoms towards the walls of the cylinder. Clearly, the solutions of the Schrödinger equation with $U_\perp^p$ as potential will always have the atomic vibrational ground state distribution peaking in the vicinity of the guide walls. As we argue below, from the point of view of atom guiding, such a dipole orientation will not result in efficient atom guiding by the TM_{11} mode with positive detuning.

Figure 8(b) is the analog of Fig. 6(b) exhibiting the variations of the potential for fixed side $b=0.6\lambda$ and increasing side a. In this case the depth of the potential in the vicinity of the walls increases with increasing a. In the limit of large a the results should converge to the parallel-plate case.

V. DYNAMIC POTENTIAL

The principal requirement of an atom guide is to efficiently confine the atoms in the axial region of the cylinder while they are acted on axially by the dissipative force. Confinement depends on the depth of the quantum well associated with the dipole potential due to the excited mode. We have so far examined the quasistatic features of this potential and we must now turn to the question of how these features

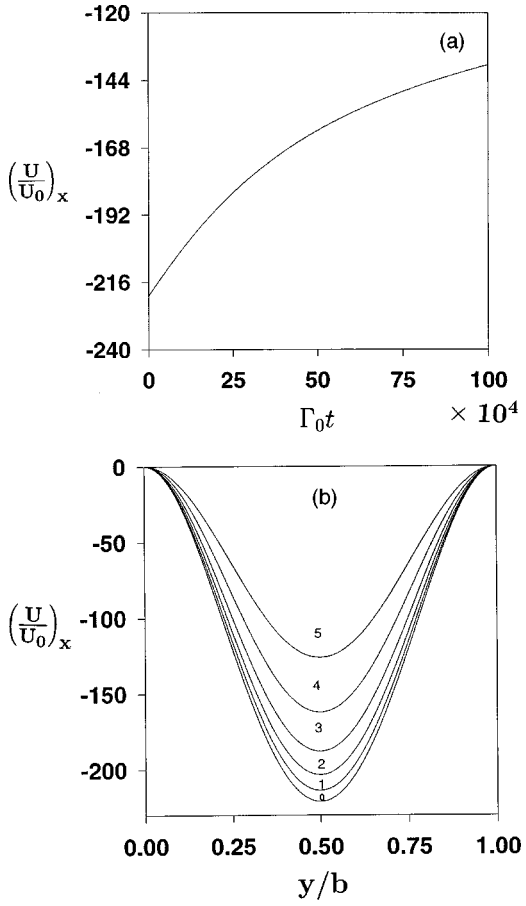

FIG. 9. Dipole along the cylinder axis (a) dynamic dipole potential at the center of the guide as a function of time; (b) variation of the potential at $x=0$, $z=a/2$ with the coordinate y for different values of the axial velocity. The labels 0–5 stand for $V_x=0.0$, 0.1, 0.25, 0.5, 1.0, and 2.0×10^4 ms^{-1}.

change with the axial motion of the atoms.

In Fig. 9(a) we display the variation of the axial potential $U_x^p(0,y,a/2,t)$ with time (measured from the instant the mode is excited). From Fig. 9(b) it can be seen that the depth of the potential well diminishes with increasing axial velocity, ultimately becoming too shallow to trap the atoms. Figure 10 displays the dipole potential $U_y^p(0,y,a/2,t)$ for different values of axial velocity when the dipole is transverse to the cylinder axis. It can be seen that the potential well becomes shallower with increasing V_x, with the region of relevant variations near the cylinder walls. Figure 11 exhibits the variation of the axial dissipative force and the corresponding axial velocity when the dipole is along the axis. It can be seen that the axial dissipative force asymptotically approaches small values, while the axial velocity tends to a constant value.

From the illustrations discussed above, it is clear that the desirable guiding action not only depends on the system parameters, but also on the dipole orientation. In order to maintain a transverse trapping capability for atoms with axial dipole orientation, the system parameters should be adjusted in such a manner resulting in a sufficient central well depth, especially at large axial velocities. With the same system parameters, we have shown that the excitation of the same waveguide mode does not result in a central dipole potential

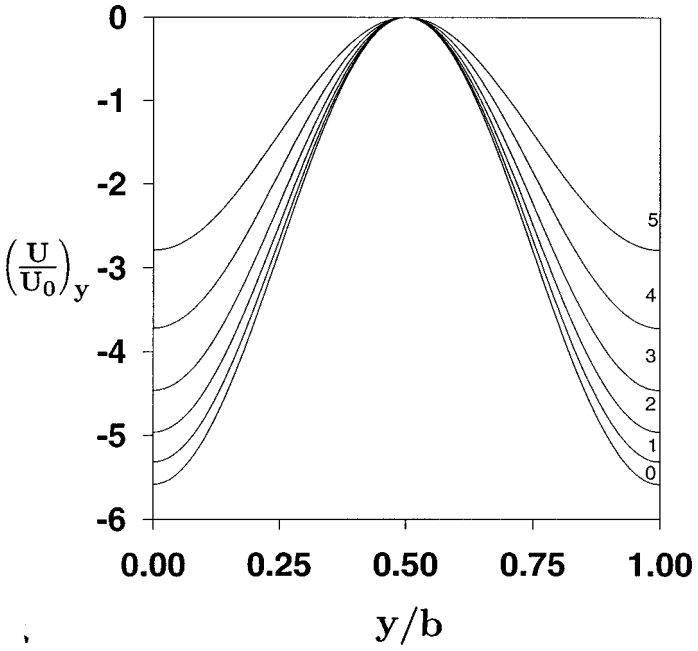

FIG. 10. Dipole transverse to the axis (along y axis): spatial distribution of the potential at $x=0$, $z=a/2$ against y for different values of the axial velocity. The labels 0–5 stand for $V_x=0.0$, 0.1, 0.25, 0.5, 1.0, and 2.0×10^4 ms^{-1}.

well when the dipole is oriented transverse to the cylinder axis, and the atoms tend to be channeled in the vicinity of guide walls.

VI. COMMENTS AND CONCLUSIONS

In conclusion we have examined in detail the properties of atoms in waveguides with rectangular cross sections. The cavity modes are first quantized, allowing the spontaneous emission rate to be evaluated for an electric dipole located at an arbitrary point. Useful limits of the spontaneous rate have been derived. In particular, we have been able to recover the results appropriate for the parallel-plate case when side a of the rectangular cross section becomes large, while side b is kept fixed. We have shown that in the limit of small cross section, especially when both a and b are less than a transition wavelength, spontaneous emission is possible only via

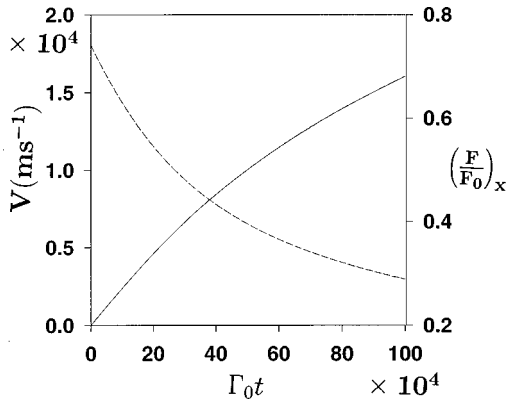

FIG. 11. Dipole along the cylinder axis: time evolution of the axial velocity (full curve) and the dissipative force acting on the atom (dashed curve).

one or two cavity modes. With a cavity mode excited, we have shown that the atoms become subject to a transverse dipole potential and an axial dissipative force, both of which vary across the cylinder and are also functions of the atom axial velocity. The dipole potential is responsible for the transverse trapping (and hence the channeling) of atoms at specific regions of the cross section, depending on the atom axial velocity and the dipole orientation, while the dissipative force controls the axial motion of the channeled atoms. The conditions facilitating atom guiding have been explored using typical parameters for sodium atoms in rectangular cylinders of subwavelength dimensions.

The most striking feature of a rectangular guide in the subwavelength regime is the depth of the well that can be achieved in comparison with that for the parallel-plate case. For the same set of parameters we have seen in [1] that the depth is of the order 211.5 MHz, while here the depth reaches 1.034 GHz, which is almost five times that of the parallel-plate well depth. Cylindrical atom guides confine atoms transversely in two directions and so have the ability to eliminate the problems of transverse diffusion that are manifest in the parallel-plate case. Additionally we have now seen that they are much more efficient atom guides on account of the depth of the central well.

We emphasize the principal property of subwavelength atom guides by contrasting this with the case of larger cylindrical atom guides with dimensions of order 10 μm. For such large dimensions the waveguide is multimode, the mode frequency separation is at least one order of magnitude smaller, and, so, spontaneous emission is effectively that in free space. This has been held to lead to the loss of guided beam coherence [5]. By contrast atom guides with subwavelength dimensions are capable of single mode operation. Also in such guides spontaneous decay occurs by emission into one or two decay channels. Experimental work on single mode guides has been reported recently by Ito *et al.* [7].

We have focused here only on cylindrical atom guides characterized by two distinct features. First the guide is assumed to have a rectangular cross section and second, the walls of the waveguide are taken to be perfect conductors. An obvious line of extension of this work should consider cylindrical perfect conductor atom guides with circular cross sections also of subwavelength dimensions. Although the spontaneous emission rate in circular cylinders has been investigated in the recent work by Rippin and Knight [18], the details of atom dynamics along the lines discussed in this paper have not yet been reported. It is well known that the electromagnetic modes of circular cylindrical guides have azimuthal components, but the significance of this property for the motion of atoms in the guide is yet to be determined. The angular momentum features associated with the mode phase should involve a light-induced torque [13] and the consequent helical motion of atoms trapped in potential rings and guided through the structure. Atom dynamics in cylindrical guides with circular cross sections of submicron dimensions is currently under investigation. A related problem that we are currently addressing is that of cylindrical atom guides with guide walls made of dielectrics characterized by dispersive dielectric functions which could also exhibit loss. A theory focusing on such features can, additionally, accommodate the first type of atom guide discussed in our previous paper [1], namely, the evanescent mode guides which can now have the new feature of the submicron dimensions. Cold atom guiding introduces new aspects which stem from two physical effects associated with slow atoms. First the quantum-mechanical nature of the vibrational states is expected to play a role in the dynamics and secondly the dipole moment of a slow atom within the guide should have sufficient time to adjust to the mode polarization. These matters will not be discussed any further here.

ACKNOWLEDGMENTS

We are grateful to E. A. Hinds and M. G. Boshier for useful discussions, and to M. Bowáaneh for his help with the computational aspects of this work. S. Al-Awfi wishes to acknowledge financial support from the Saudi Arabian government.

[1] S. Al-Awfi and M. Babiker, Phys. Rev. A **58**, 2274 (1998).
[2] J. P. Dowling and J. Gea-Banacloche, Adv. At., Mol., Opt. Phys. **37**, 1 (1996).
[3] M. J. Renn, D. Montgomery, O. Vdovin, D. Z. Anderson, C. E. Wieman, and E. A. Cornell, Phys. Rev. Lett. **75**, 3253 (1995).
[4] M. A. Ol'Shanii, Y. B. Ovchinnikov, and V. S. Letokhov, Opt. Commun. **98**, 77 (1993).
[5] S. Marksteiner, C. M. Savage, P. Zoller, and S. L. Rolston, Phys. Rev. A **50**, 2680 (1994); C. M. Savage, D. Gordon, and T. C. Ralph, *ibid.* **52**, 4741 (1995).
[6] W. Jhe, M. Ohtsu, H. Hori, and S. R. Freiberg, Jpn. J. Appl. Phys., Part 2 **33**, L1680 (1994).
[7] H. Ito, K. Sakaki, T. Nakata, W. Jhe, and M. Ohtsu, Opt. Commun. **115**, 57 (1995); H. Ito, K. Sakaki, M. Ohtsu, and W. Jhe, Appl. Phys. Lett. **70**, 2496 (1997).
[8] M. J. Renn, E. A. Donley, E. A. Cornell, C. E. Wieman, and D. Anderson, Phys. Rev. A **53**, R648 (1996).
[9] The modes are well known from microwave theory and the derivation can be found in any suitable text on electromagnetic theory. See also R. E. Collin, *Field Theory of Guided Waves*, 2nd ed. (IEEE, New York, 1991), Chap. 5.
[10] G. Barton, Proc. R. Soc. London, Ser. A **320**, 251 (1970); **410**, 141 (1987); **410**, 175 (1987); **453**, 2461 (1997).
[11] E. A. Hinds, Adv. At., Mol., Opt. Phys. **28**, 237 (1990).
[12] C. S. Adams and E. Riis, Prog. Quantum Electron. **21**, 1 (1997).
[13] M. Babiker, W. L. Power, and L. Allen, Phys. Rev. Lett. **73**, 1239 (1994).
[14] L. Allen, M. Babiker, V. E. Lembessis, and W. K. Lai, Phys. Rev. A **54**, 4259 (1996).
[15] C. I. Sukenik, M. G. Boshier, D. Cho, V. Sandoghdar, and E. A. Hinds, Phys. Rev. Lett. **70**, 560 (1993).
[16] V. Sandoghdar, C. I. Suknik, S. Haroche, and E. A. Hinds, Phys. Rev. A **53**, 1919 (1996).
[17] V. Sandoghdar, C. I. Sukenik, E. A. Hinds, and S. Haroche, Phys. Rev. Lett. **68**, 3432 (1992).
[18] M. A. Rippin and P. L. Knight, J. Mod. Opt. **47**, 807 (1996).